Desalination and Water Treatment
www.deswater.com

doi: 10.5004/dwt.2020.24686

173 (2020) 86–104
January

Performance and cost assessment of a solar HDH desalination system integrated with thermal storage: a case study

M. Ifras Zubair[a], Fahad A. Al-Sulaiman[a,b,*], Mohammed A. Antar[a], S. Dini[a], Nasiru I. Ibrahim[b]

[a]*Mechanical Engineering Department, King Fahd University of Petroleum and Minerals, Dhahran 31261, Saudi Arabia, email: m.i.zubairs@gmail.com (M. Ifras Zubair), Tel. +966-13-860 2964; email: antar@kfupm.edu.sa (M.A. Antar), Tel. +966-13-860 7028; email: ahsalem@kfupm.edu.sa (S. Dini)*

[b]*Center of Research Excellence in Renewable Energy, Research Institute, King Fahd University of Petroleum and Minerals, P.O. Box: 5040, Dhahran 31261, Saudi Arabia, Tel. +966-13-860 7322; Fax: 966-13-860 7312; email: fahadas@kfupm.edu.sa (F.A. Al-Sulaiman), Tel. +966-13-860 8472; email: nasiru@kfupm.edu.sa (N.I. Ibrahim)*

Received 3 February 2019; Accepted 10 July 2019

ABSTRACT

Solar desalination systems often have limited operating hours and their operation is significantly affected by the variation of solar radiation intensity. A model of a humidification–dehumidification (HDH) desalination system integrated with evacuated tube solar collectors and thermal storage is developed and validated against available data in the literature. Operating parameters such as the maximum temperature of water heater and the mass flow rate ratio of the HDH component are optimized. The thermal storage unit consists of separate hot and cold-water storage tanks, which allow control of the water temperature leaving the storage unit. Furthermore, performance of the system for six different geographical locations in Saudi Arabia, namely Riyadh, Jeddah, Dhahran, Qassim, Sharurah, and Tabuk, is studied. The system is evaluated for four different scenarios as follows: (i) 24-h operation; (ii) with the ideal flow rate; (iii) with the average flow rate; and (iv) with the maximum flow rate. The effect of flow rate on the number of operating hours and the rate of freshwater production is also evaluated. The maximum freshwater production is 9.346 L/h and the minimum is 3.01 L/h. For a service life of 20 years, the cost of freshwater produced varies from 0.021 to 0.034 $/L considering interest rate of 2%.

Keywords: Solar energy; Humidification–dehumidification; Desalination; Clean water; Thermal storage tank; Constant freshwater output

1. Introduction

Scarcity of fresh-drinking water is persisting globally, affecting mainly dry regions and desert areas. However, a common advantage in such areas is the availability of abundant solar radiation. The use of solar energy to produce freshwater in such regions is one of the viable solutions to address the scarcity of freshwater. Other means of supplying water to those regions is by transporting desalinated water or conveying water from natural sources. However, this is tremendously costly, and it might not be cost-effective considering small populations in rural areas [1]. A common issue faced with these systems is the variation in productivity due to changes in the availability of solar radiation. A solar desalination system with an integrated thermal storage option can provide a small-scale and constant production and supply of freshwater on demand.

* Corresponding author.

About 65% of the entire world's desalination market employs the reverse osmosis technique, while the rest uses thermal desalination processes [2]. Solar stills and humidification–dehumidification (HDH) processes are among the widely used thermal desalination techniques. These techniques operate at low temperatures as a result of the differences in the quantity of water vapor in the air stream [3]. Solar still is an equipment which carries out thermal desalination process that requires a larger solar collector area due to its significant low performance and production [4]. This is because the technique combines all processes into a single unit operating as a complete system. These combined processes are evaporation, condensation and water heating within the solar thermal collection [5]. The performance of solar stills relies on solar radiation, cloud cover, ambient temperature and wind speed. The output of these systems may also be affected by factors such as brine depth, insulation and vapor leakage [6].

HDH desalination systems when compared with solar stills have significantly higher gain output ratio (GOR), thereby requiring a comparatively smaller area for solar energy collection. The required technical support and capital investments associated with HDH desalination systems are minimal, as it involves simple mechanisms and can operate with raw water of varying quality [7,8]. The maintenance procedures involved are also far less complicated [9].

HDH systems in general include components such as, heat supply systems, condensers, and evaporators along with an option for thermal storage. The process involves direct contact between warm saturated air and warm raw water allowing the air to reach a preferred humidity level, which is followed by extraction of water vapor from the humid air using a condenser to generate freshwater [10]. The main factors affecting evaporation and condensation of an HDH system are the rate of evaporation of water and condensation, and the temperature of the cooling water. The rate of evaporation of water and condensation increases with increasing amount of evaporative raw water and its inlet temperature [11]. The condensation rate is also higher at lower cooling water temperature [12].

As desalination and cooling systems in general require huge amount of energy to operate, most of these systems are in operation at locations where solar energy is abundant (deserts or high temperature zones). The integration of solar energy with these systems is a major advantage to provide the supply to meet the increasing demand for such systems [13]. Kim and Seo [14] proved that the performance of different type of evacuated tube collectors depends on the type and arrangement of the absorber tubes. They showed that a U tube on a copper absorber plate provides best results. Ng and Khor [15] evaluated the thermal losses of an ETC with a heat pipe design and concluded that there are radiation heat losses between the absorber and the ambient environment, losses at the manifold, and thermal resistance losses within the collector. In terms of choice between water heating and air heating for HDH systems, Yildirim and Solmus [16] showed that water heaters have significantly better freshwater production as compared with air heated systems, owing to the higher heat capacitance of water as compared with air. A similar system was also studied theoretically and experimentally where both air and water are heated by two solar collectors [17]. Kabeel and El-Said [18,19] investigated numerically and experimentally a hybrid HDH/flash evaporation desalination system, employing solar air and water heaters. The results showed that the productivity of the system increases with increase in the temperature of feed water and the air mass flow rate. The authors also reported a comparative study of different configurations of the hybrid system [20].

In order to minimize the initial cost of investment and space requirement for incorporating two separate solar collectors as in the study by Yildirim and Solmuş [16], and Rajaseenivasan and Srithar [21] studied the feasibility of using a dual purpose solar collector for simultaneously heating both air and water in a HDH system. The results indicate that the system capacity increases with the flow rate of air and water. Wu et al. [7] showed that minimum work required in the HDH process is about 100.21 kJ for every production of 1 kg freshwater when the ideal HDH desalination system operates at 303 K and at ambient temperature of 293 K. Kabeel et al. [22] reported an experimental study on an open-water and closed-air HDH system powered by evacuated tube collectors without storage. The authors later modeled the same system and showed that the total cost of freshwater from the unit is 0.0578$/l [23]. Other researchers applied vapor compression heat pump for water desalination based on HDH configuration [24–26].

Energy storage is needed for uninterrupted operation of solar powered thermal systems including HDH due to the intermittency of the solar energy. Based on heat storage mechanism, thermal energy storage is classified into sensible heat, latent heat and thermochemical heat storage [27]. The extent of availability of solar radiation, expected loads, type of auxiliary energy, economic feasibility, the rate of solar energy required to substitute conventional energy used, and the required reliability are some of the main factors that affect the optimum capacity of thermal storage [28].

Latent heat storage depends on phase changes of materials from solid to liquid, liquid to gas and vice versa. Phase changing process is isothermal, indicating that the temperature of the storage material does not change. Latent heat storage usually operates within small temperature ranges and has high storage capacities with relatively low mass and volume [28]. Shabaneh et al. [29] suggested that tilted solar air heaters account for about 7% higher performance, with the performance of the humidifier largely impacting system productivity. Summers et al. [30] pointed out that a constant heating temperature and constant heat output are important for HDH cycle performance. The use of phase change materials (PCM) was shown to provide consistent air outlet temperatures through day and night. In the proposed design, the PCM was placed just below the absorber plate.

The technology of thermal storage using PCMs is considered as one of the most useful thermal storage options, due to the constant temperature in storing and releasing heat, high density of heat storage, and ease of control. Heat storage and release in this type of systems is affected by the flow rate at the inlet and outlet of the storage component. During the day time if the temperature of the collector outlet exceeds the maximum allowed temperature, additional heat is directed to the thermal storage unit [31]. Wang et al. [32] investigated the economic feasibility of solar desalination

system with PCM storage at different locations and means of promoting such systems by subsidies and promotional activities in dry regions.

A hybrid spray flash system combined with latent heat storage can be used to develop an energy saving desalination system that stores thermal energy from solar heat, waste heat, and the surplus steam of a power station. The stored energy can be used not only for air conditioning and power generation but also for freshwater production. Experimental results obtained by Miyatake et al. [33] on heat storage by the use of PCMs shows that efficiency rates of the hybrid system are high (around 95%). Shalaby et al. [34] recommended the use of PCM as thermal energy storage medium to maintain near constant temperature of the feed water during the day and to ensure 24 h/d system operation.

On the other hand, the high heat capacity of water makes it a good candidate as thermal storage medium for applications that require heating and cooling, although large quantities of water are required due to its lower storage density. Water storage tanks are highly recommended for 24-h operation of humidification–dehumidification desalination plants. Storage materials such as rocks or ceramics have the capability of maintaining large temperature differences; however they have a relatively low heat capacity [35].

Muller-Holst et al. [36] found that the performance of multi-effect humidification desalination systems with thermal storage can be maintained for over 5 years without extensive maintenance. They showed that the cost could be reduced by more than 50% by the addition of a storage system. They also showed that the cost of freshwater production could be reduced by a further 20% with better evaporation surfaces and thinner flat plate heat exchangers. Abd El-Aziz et al. [37] compared two HDH systems; one with thermal storage and the other without storage and found considerable reduction of the cost of water production due to storage. Srithar and Rajaseenivasan [38] considered hot water storage coupled with solar collector for continuous supply of fresh water from a HDH system. They performed numerical simulation and studied the effects of three different configurations of the hot storage on freshwater production.

Literature review indicates that research on humidification–dehumidification desalination systems powered by solar thermal collectors and coupled with thermal storage options are rare. For example, the literature [32–34] focused on the integration of latent heat storage while Srithar and Rajaseenivasan [38] considered hot water storage. This paper introduces a unique energy storage system that uses hot and cold storage tanks as two separate storage entities to provide constant heat input to the HDH system. Such an approach is expected to smoothen the fluctuations of energy input through renewable sources, where the diurnal variations of the heat gained through collectors can introduce thermal stresses and irregular water production rates. The design proposed in this study introduces a water-heated HDH system that uses evacuated tube collectors for thermal energy collection, along with thermal storage as part of a master thesis [39]. The humidifier and dehumidifier units of the system used packed beds that provide good efficiency of about 85% for the evaporation and condensation components. Detailed thermodynamic analysis was conducted to evaluate the performance of the proposed system, with the performance evaluation conducted for Dhahran, Saudi Arabia. Furthermore, the analysis was extended, and the performance of the proposed system was evaluated at six different locations in Saudi Arabia.

2. Methods

2.1. System description

The proposed design is a closed-air/open-water (CAOW) HDH system, integrated with an evacuated tube water heater and a unique thermal storage system as shown in Fig. 1. A closed-loop air system design was chosen because it has higher performance as compared with the open-air HDH system. The thermal storage system is designed to provide a 24-h operation and freshwater production at a constant rate, by providing saline water to the humidifier at a constant temperature. Heat is added to saline water exiting the dehumidifier to maintain the constant temperature,

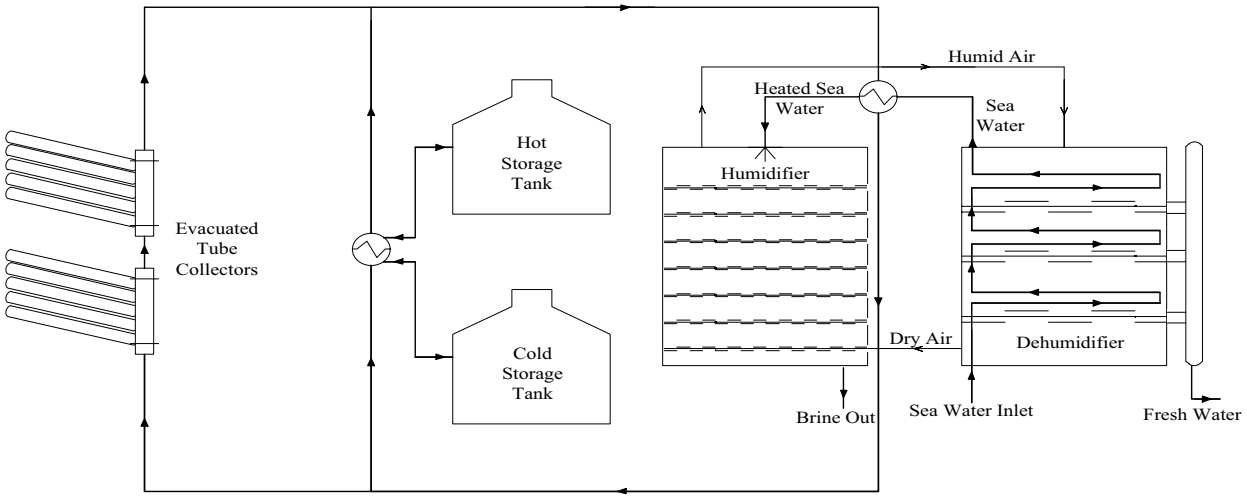

Fig. 1. System schematic [39].

by the combination of hot and cold storage tanks through an integrated control system. The system would maintain a constant temperature as required, providing smooth operation of the desalination plant as well as controlling its operation depending on the time of the day. The fluid used within the collector may have special properties in order to improve the thermal energy collection and prevent boiling or freezing. This is possible due to the use of a heat exchanger, which does not involve direct mixing with the heating fluid. The heating fluid considered in this study is water.

Several modeling assumptions are considered as reported in the study by Zubair et al. [40] as follows:

- The system is studied under steady-state conditions on hourly basis variation.
- No leakage of water or air occurs within the system such as humidifier, dehumidifier, and solar collector [41,42], and the system is assumed insulated.
- The energy balance equations consider incompressible flow and neglect pressure drop.
- The freshwater leaving the dehumidifier is at the average temperature between the dew-point temperature of the inlet air and the dry-bulb temperature of the exit air from the dehumidifier [43].
- The collector receiver area is assumed to be at a uniform temperature.
- The temperature gradients across the plate thickness and along the perimeter are negligible.
- Thermal resistance due to contact between the receiver area and the evaporator section, and the manifold and the condenser, is negligible.
- The joints between the evaporator heat pipe and the condenser are assumed adiabatic.

2.2. Mathematical model

The mathematical modeling is conducted for the solar collector, the humidification–dehumidification cycle, and the thermal storage system as presented in the following sections.

2.2.1. Evacuated tube collector

The absorbed radiation (S) is given by the following equation [28]:

$$S = I_b R_b \left(\tau\alpha\right)_b + I_d \left(\tau\alpha\right)_d \left(\frac{1+\cos\theta}{2}\right) + \rho_{gr} I \left(\tau\alpha\right)_{gr} \left(\frac{1-\cos\theta}{2}\right) \quad (1)$$

The heat transfer balance across the ETC is given by the following equation [44]:

$$Q_{in} = Q_{loss,rad} + Q_{hp} = Q_{loss,rad} + Q_u + Q_{loss,ma} \quad (2)$$

Reference to Eqs. (1) and (2) and Fig. 2, the radiation (S) is absorbed by the receiver of the ETC, and a relatively small portion of it is lost through radiation, $Q_{loss,rad}$. Q_u is the useful heat gain of the thermal collector, which is obtained by the difference between the heat pipe gain (Q_{hp}) and the $Q_{loss,ma}$ known as the manifold heat loss. The radiation and manifold losses are calculated considering the radiation theraml resistance and manifold resistances, respectively, based on the formulation presented in the study by Jafarkazemi and Abdi [44].

The useful energy of the collector Q_u can also be rewritten as follows [28]:

$$Q_u = A_r F_R \left[S - U_L \left(T_i - T_a\right)\right] \quad (3)$$

where F_R known as the collector heat removal factor is given by the following equation [28]:

$$F_R = \frac{\dot{m} C_p}{A_r U_L}\left[1 - \exp\left(-\frac{U_L A_r F'}{\dot{m} C_p}\right)\right] \quad (4)$$

In addition, Q_u is defined as the energy extracted by the collector working fluid as:

$$Q_u = \dot{m} C_p \left(T_f - T_0\right) \quad (5)$$

The ratio of useful energy to the absorbed solar radiation is known as the efficiency of the collector, which is given by the following equation [44]:

$$\eta = \frac{Q_u}{A_r I_T} = F_R \left(\tau\alpha\right) - \frac{F_R U_L \left(T_i - T_a\right)}{I_T} \quad (6)$$

where I_T is the total radiation available to the collector.

2.2.2. Humidification–dehumidification system

Energy balance equations were evaluated for the humidifier, dehumidifier and the solar water heater as follows [43]:

Humidifier

$$\dot{m}_w h_{w3} + \dot{m}_a h_{a1} = \dot{m}_b h_{w4} + \dot{m}_b h_{a2} \quad (7)$$

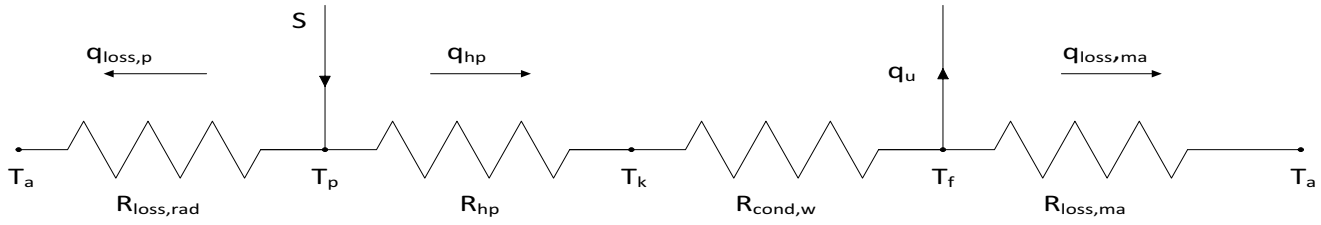

Fig. 2. Thermal circuit of an evacuated collector tube.

In which, h_{a1} – enthalpy of air at the exit of the dehumidifier or the inlet of the humidifier.

Dehumidifier

$$\dot{m}_w\left(h_{w2}-h_{w1}\right)+\dot{m}_{\mathrm{fw}}h_{\mathrm{fw}}=\dot{m}_a\left(h_{a2}-h_{a1}\right) \tag{8}$$

Solar water heater

$$Q=\dot{m}_w C_{\mathrm{pw}}\left(T_{w3}-T_{w2}\right) \tag{9}$$

The effectiveness of the humidifier and the dehumidifier is given by the following equation:

$$\eta=\frac{\Delta\dot{H}}{\Delta\dot{H}_{\max}} \tag{10}$$

The mass flow rate of fresh water is defined by the humidity ratios of the outlet and inlet of the humidifier, as follows:

$$\dot{m}_{\mathrm{fw}}=\dot{m}_a\left(w_2-w_1\right) \tag{11}$$

in which, ω_2 – absolute humidity of air at the exit of the humidifier and the inlet of the dehumidifier,

ω_1 – absolute humidity of air at the exit of the dehumidifier and the inlet of the humidifier.

The flow rate of brine is then found by subtracting the flow rate of fresh water from the flow rate of water entering the system:

$$\dot{m}_b=\dot{m}_w-\dot{m}_{\mathrm{fw}} \tag{12}$$

The performance of an HDH system, known as the gained output ratio (GOR), is defined as follows:

$$\mathrm{GOR}=\frac{\dot{m}_{\mathrm{fw}}h_{\mathrm{fg}}}{Q_u} \tag{13}$$

The recovery ratio, defined as the ratio between fresh water and the raw water input, is shown as follows:

$$\mathrm{RR}=\frac{\dot{m}_{\mathrm{fw}}}{\dot{m}_{\mathrm{sw}}} \tag{14}$$

2.2.3. Thermal storage

Thermal storage consists of a hot storage tank and a cold storage tank, where the hot storage tank is considered as an un-stratified water storage unit. When heat is demanded by the HDH, the control system measures the hot storage tank temperature and water from the cold storage is mixed with water from the hot storage at the heat exchanger to provide the required temperature to the water line between the humidifier and the dehumidifier. Temperature of the storage at the end of the time period, T_s^+, is defined by the following equation:

$$T_s^+=T_s+\frac{\Delta t}{\left(mC_p\right)_s}\left\{\begin{array}{l}A_cF_R\left[S-U_L\left(T_s-T_a\right)\right]^+-\left(\mathrm{UA}\right)_s\left(T_s-T_a'\right)-\\ \varepsilon_L\left(\dot{m}C_p\right)_{\min}\left(T_s-T_{\mathrm{Lr}}\right)\end{array}\right\} \tag{15}$$

where $(\mathrm{UA})_s$ – storage tank loss coefficient area product and A_c is the collector area.

The model equations were evaluated to simulate the proposed design, using the engineering equation solver software (EES).

2.2.4. Validation

The engineering equation solver (EES) software uses a numerical iterative method to solve equations simultaneously. The condition for convergence is that the residuals of equations should be smaller than 10^{-6} or the change in variables is less than 10^{-9} as shown in Fig. 3. The data used for the calculations as input parameters are the hourly incident solar radiation on a horizontal surface in (MJ/m^2), ambient temperatures in kelvin, and the latitude for the chosen location. The calculations were performed for Dhahran, Saudi Arabia. Pure water properties ware used in the calculation instead of seawater properties, because this does not significantly affect the performance of the HDH cycle according to the literature [26].

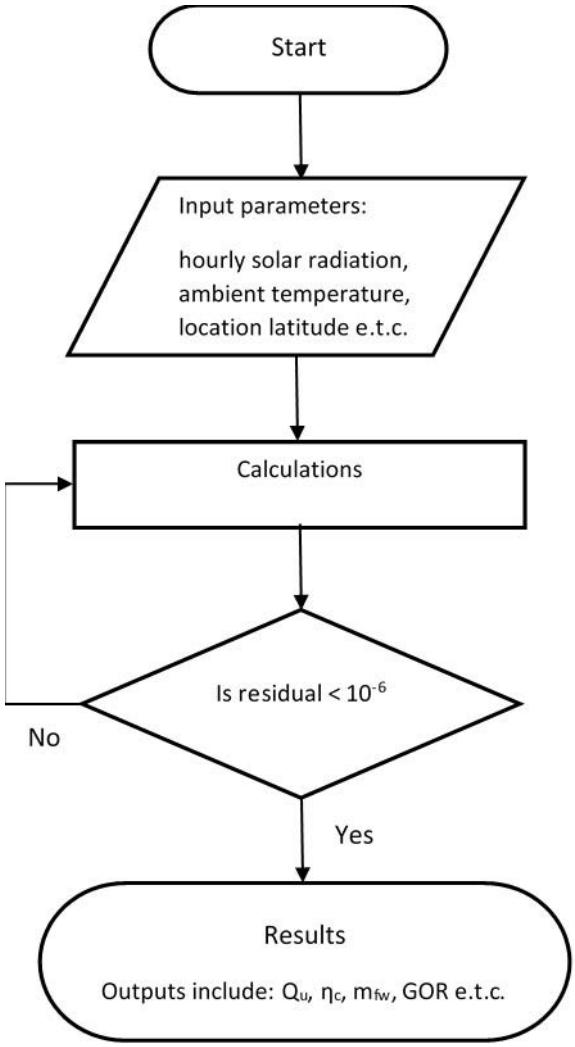

Fig. 3. Calculation flow chart.

2.2.4.1. Evacuated tube collector

Mathematical models were formulated for the evacuated tube solar collector and the HDH system separately. The collector was modeled as a water heater, whereas the HDH system was modeled as a closed-air/open-water system with a source of heated water.

The comparison shown in Table 1 is for collectors with the highest output capacity using the lowest collector area. The cost comparison is based on an average price of \$500/m^2 of the collector, Table 1. Data for Apricus AP-30 evacuated tube collector, which is the collector with the highest productivity, is shown in the first row of the table. This collector is shown to have the highest capacity for the gross area and the estimated cost is nearly the same as the actual purchase price, which was later found to be \$1,930 [45]. Thus, the calculations show that the value for the capital spent is received.

The main parameter used to validate the code for the evacuated tube collector is the efficiency of the collector. A comparison between the calculated collector efficiencies and the measured efficiencies obtained from technical information provided by the manufacturer as a function of the operating temperature is shown in Table 2. The comparison, performed for temperatures in the range of 50°C–80°C, is well within the expected temperature limits of this system [46]. The measured and calculated efficiencies of the ETC agree within experimental error.

2.2.4.2. Humidification–dehumidification desalination system

Sharqawy et al. [43] presented a design example for a CAOW HDH desalination system. The authors used inputs such as the GOR (1.93), the recovery ratio (0.0306), the latent heat of vaporization (2,345 kJ/kg K), along with the mass ratio (2.04) to calculate the relevant air and sea water flow rates and the required heat input, which are given in Table 3. The table also shows the results obtained with the proposed model, which are in good agreement with the values reported by Sharqawy et al. [43]. This validates the HDH model presented in this paper.

The results obtained from the proposed model were also validated by comparing with the results reported by Narayan et al. [47]. They evaluated the effect of relative humidity of air at the inlet and exit of the humidifier on the performance of a HDH system as measured by GOR. The values of the variables used in the evaluation are shown in Table 4.

Fig. 4 shows the effect of relative humidity on the performance of an HDH system, a comparison between the

Table 1
Evaluation of the collectors

Manufacturer	Model	Gross area per collector (m^2)	Cost per unit	Capacity (kW)	Capacity per dollar	Capacity/ Gross area
Apricus	Arpicus AP-30	4.05	\$1,900	2.66	0.0014	0.65679
Calpak	16 VTN	2.86	\$1,430	1.83	0.00128	0.63986
Ritter Solar	CPC 30 Star Azzurro	3.30	\$1,651	2.11	0.00128	0.639394
Calpak	6 VTN	1.06	\$530	0.67	0.00126	0.632075
Oventrop	OV 5-8 AS/AB	2.03	\$1,014	1.28	0.00126	0.630542
Ritter Solar	CPC 14 Star Azzurro	2.61	\$1,305	1.63	0.00125	0.624521
Beijing Sunda Solar Energy Technology	Seido 10-20 AS/AB	3.39	\$1,697	2.11	0.00124	0.622419

Table 2
Validation of the model for the evacuated tube collector at 800 W/m^2 irradiation

$\Delta T = (T_{mean} - T_a)$	Measured efficiency[a]	Calculated efficiency	Deviation (%)
50°C	0.6	0.59	1.67
60°C	0.58	0.57	1.72
70°C	0.54	0.53	1.85
80°C	0.51	0.5	1.96

[a]From technical information provided by the manufacturer [46].

Table 3
Validation of the proposed HDH model by comparison with the results of Sharqawy et al. [43]

Calculated variables	Literature values	Model values	Deviation (%)
Q_{in}	3.34 kW	3.37 kW	0.90
m_w	0.0899 kg/s	0.0907 kg/s	0.89
m_a	0.0442 kg/s	0.0445 kg/s	0.68

Table 4
Values of the variables used by Narayan et al. [47] to assess the effect of relative humidity of air

Variable name	Value
Dehumidifier effectiveness	90%
Humidifier effectiveness	90%
Mass flow of air	0.1 kg/s
Mass flow of water	0.5 kg/s
Mass ratio	5
Maximum temperature	80°C
Minimum temperature	35°C

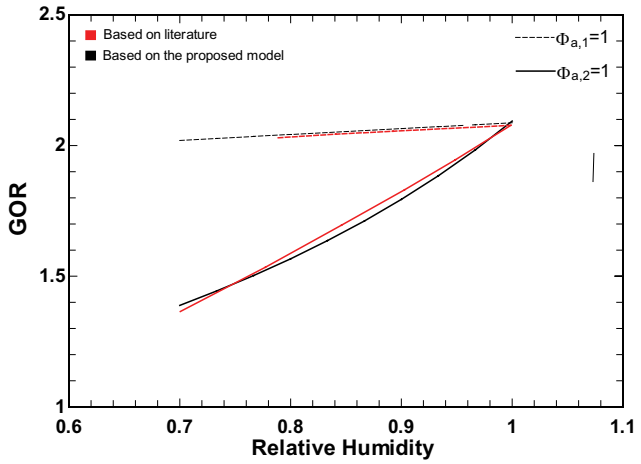

Fig. 4. Comparison of GOR vs. relative humidity plot obtained using the proposed model with that reported by Narayan et al. [47].

graph reported by Narayan et al. [47] and the graph produced via EES for the proposed HDH desalination system model. $\phi_{a,1}$ and $\phi_{a,2}$ are the humidity ratios of air at the exit and inlet of the humidifier, respectively. As reported in the literature, varying the relative humidity of air at the exit of the humidifier between 70% and 100% changes GOR by about 3%, which is shown by the red dashed line in Fig. 4. The black dashed line in the figure represents the results obtained through EES using the model under similar conditions. The two lines are in good agreement, with the calculations based on the proposed model also showing an approximately 3% change in GOR. The solid red line represents the effect of changing the relative humidity of air at the inlet of the humidifier on GOR, as reported in the literature, showing a much greater effect on the performance (34%). The black solid line represents the variation in GOR calculated using the proposed model under similar conditions. The two lines are in good agreement, with a variation in performance of about 31%, which validates the proposed model.

The proposed model was further validated using the comparison of the plot of mass flow rate ratio, MR (mass flow of water to air) vs. GOR obtained using the model with that reported by Sharqawy et al. [43] as shown in Fig. 5. The two curves in the figure are calculated based on

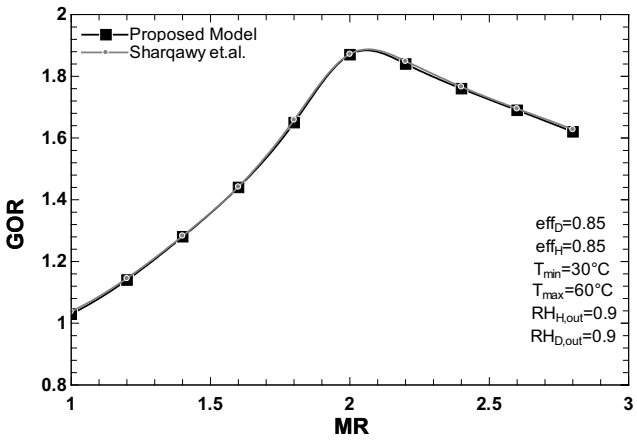

Fig. 5. Comparison of GOR vs MR plot obtained using the proposed model with that reported by Sharqawy et al. [43].

similar conditions. The two curves are very similar, with GOR reaching a maximum close to an MR value of approximately 2. The GOR increases until a maximum and gradually declines as the air-to-seawater flow ratio is inadequate to further increase the productivity of the HDH system. The effectiveness of both the dehumidifier and the humidifier is 0.85, and the relative humidity is 0.9. The figure shows the existence of an optimum mass flow rate ratio for given operating conditions, in order to maximize GOR. The optimal mass flow ratio is one that allows the spray of an adequate amount of water within the humidifier in order to humidify the air to its optimal level, for a humidifier with an effectiveness of 85%.

In summary, the close agreement of the results obtained using the proposed model for the evacuated tube collector and the HDH system with those reported in the literature, demonstrates the validity of the model. Thus, it can be used to simulate the operation of a water-heated CAOW humidification–dehumidification desalination system.

3. Results and discussions

3.1. Optimization

For the optimization of the HDH system, the seawater inlet temperature is assumed constant at 25°C throughout the year. Fig. 6 shows the plots of GOR vs. MR for the HDH model indicating the optimum mass flow ratio to attain the highest GOR. The highest temperature of seawater is at the inlet of the humidifier and the advantage of the HDH systems is that they operate at low temperatures. The maximum temperature range studied is from 60°C to 80°C. The shape of the curves in the figure is due to reasons previously explained under the validation section. The figure indicates that a higher freshwater output may be obtained with a maximum temperature of 60°C. It shows an optimum value of MR of 1.8 which correspond to the highest GOR value of approximately 1.6, hence, maximum productivity with a minimum amount of heat input. The ability to use a lower maximum temperature is advantageous as it reduces scale formation around the water heater.

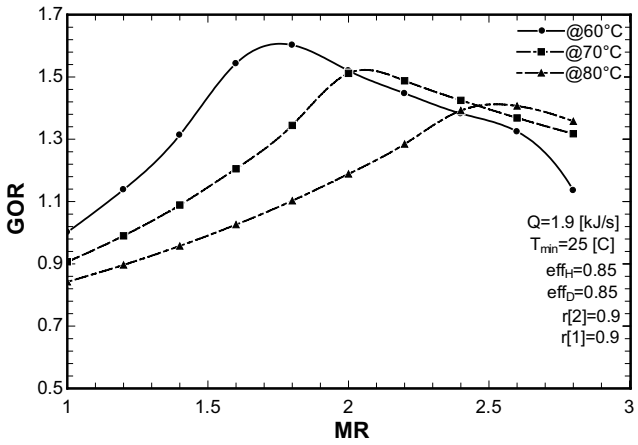

Fig. 6. Plots of GOR as a function of MR used for optimization.

The specific heat input required for the optimized conditions was used to find the number of collectors required. Two Apricus AP-30 collectors are needed to generate the required heat input for the system to produce an average of 4 L of fresh water per hour with the indicated GOR at an average value of the solar radiation. Fig. 7 shows the effect of the area of the collector on the amount of freshwater produced, which indicates that the daily total freshwater production linearly increases with the increasing number of tubes in the evacuated tube collector. Six different collector sizes are considered, through the combination of collectors containing 10, 20, and 30 tubes. The figure also shows the variation of performance of the system in four different months of the year representing the four main seasons in a year. The effects of the four seasons and the solar radiation variation are discussed later. As expected, a system with a smaller collector area operating under high solar radiation produces a similar output to that of a system containing a collector or combination of collectors with a larger area under lower solar radiation.

3.2. Direct solar HDH system

A direct solar HDH system operating in Dhahran, Saudi Arabia, from 8 am to 3 pm was employed to study the effects of the humidifier–dehumidifier effectiveness on the performance of the system. Fig. 8 shows the operation of the system for the month of June indicating the accumulated freshwater output at each hour as a function of the time of the day. As the incident radiation level is directly related to the time of day, the first point at 8 am and the last point at 3 pm have considerably lower radiation levels, as compared with the radiation level of 3.539 MJ/m^2 at 12 noon. The figure also shows that the productivity increases significantly when the effectiveness is increased from 0.85 to 0.95. However, effectiveness values above 0.85 are purely theoretical and are yet to be achieved practically. Nonetheless it proves that an increase of the effectiveness significantly increases the freshwater production. Although effectiveness values above 0.85 may be achieved by using larger humidifiers and dehumidifiers with greater packing heights, cross sectional area, etc., the exponential increase in the required capital investment cannot be justified by the expected increase in productivity. Two separate units would be cheaper to construct and will produce equal or more freshwater with a seemingly lower capital cost.

The daily average amount of freshwater produced over a year is represented by a bell-shaped curve, as shown in Fig. 9. Expected radiation values are lower at the beginning and end of the year, where the day is quite short, and the number of daylight hours is considerably lower in

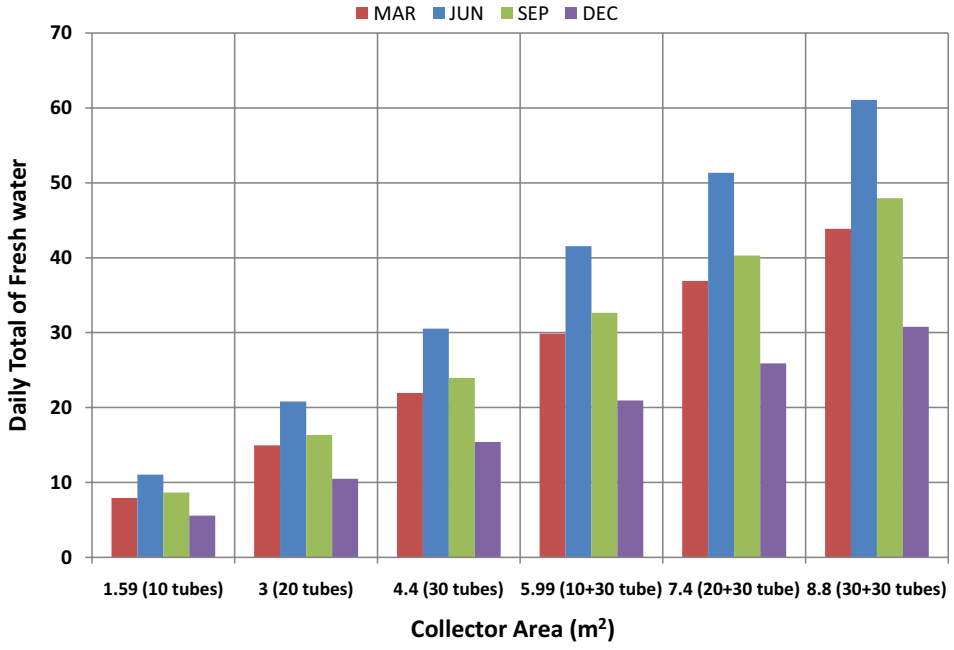

Fig. 7. Daily total freshwater output as a function of the collector area.

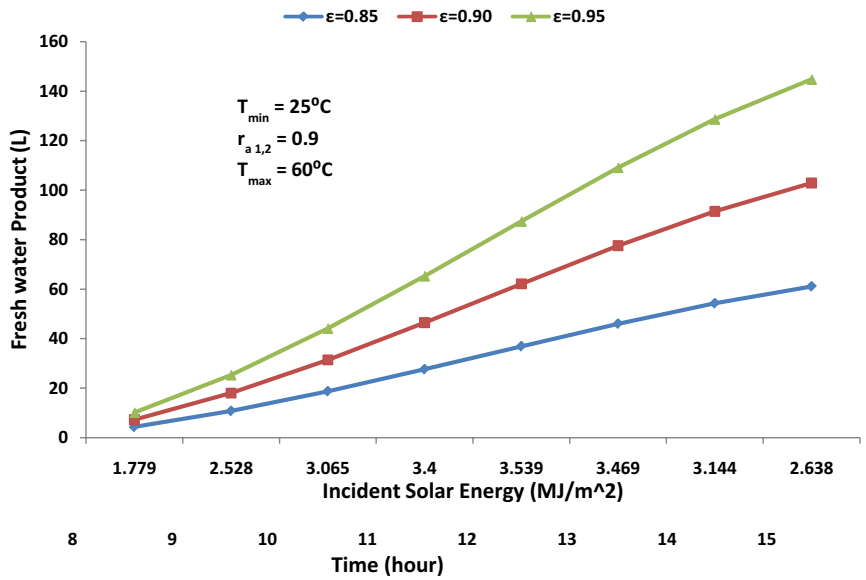

Fig. 8. Accumulated total freshwater production as a function of the time of the day for June.

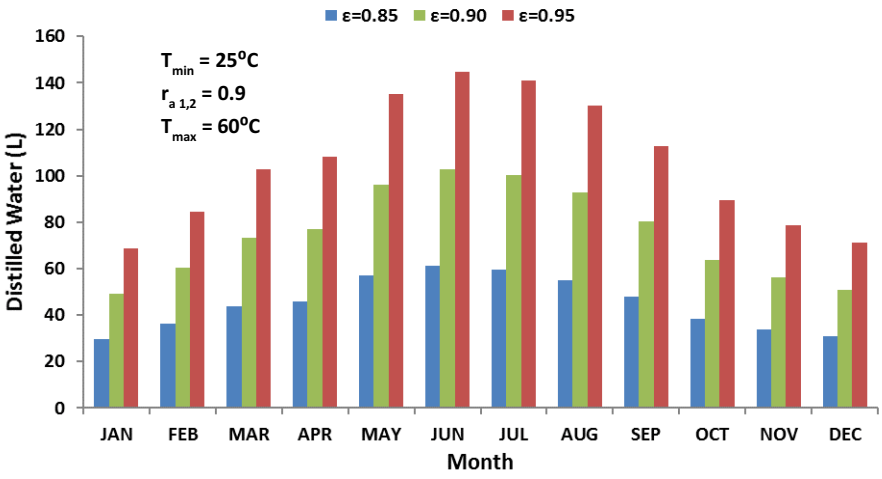

Fig. 9. Daily averaged productivity for each month of the year.

comparison with that towards the middle of the year. June has the highest recorded radiation values and the highest productivity. The seawater inlet temperature is assumed to be constant at 25°C, and the cold-water effects are not considered, which may affect positively on the productivity increment if it is considered. The daily averaged productivity follows the trends of the prevailing weather, where longer days are reported in the summer and relatively shorter days in the winter, spring, and autumn. As expected, the variation of the daily averaged GOR over the course of the year shown in Fig. 10 follows a similar trend. The GOR is computed as an average per day on each average day of every month.

3.3. System performance analysis

The storage fluid considered in this study is water, mainly due to its high thermal capacity and availability, which reduces cost of operation of the system. The standard storage capacity commonly employed in practice is 75 L/m^2 of collector area, which is also used in this study to calculate the size of storage required (660 L/175 US gallons). The closest fitting tank according to the size, along with a built-in heat exchanger, is also available from Apricus. The cost of the total system can be reduced by obtaining the collectors and the storage tank from the same manufacturer due to the availability of package deals. This issue will be further discussed later in the section on cost analysis.

The main objectives of the addition of a storage system are to attain continuous operation, maintain a constant output, enhance the productivity, and possibly lower the cost of freshwater production. The main parameter that determines the operating hours of this system was found to be the flow rate of the storage fluid to and from the storage tank. Although a higher flow rate adds more heat to the system in a shorter time, it also removes heat equally

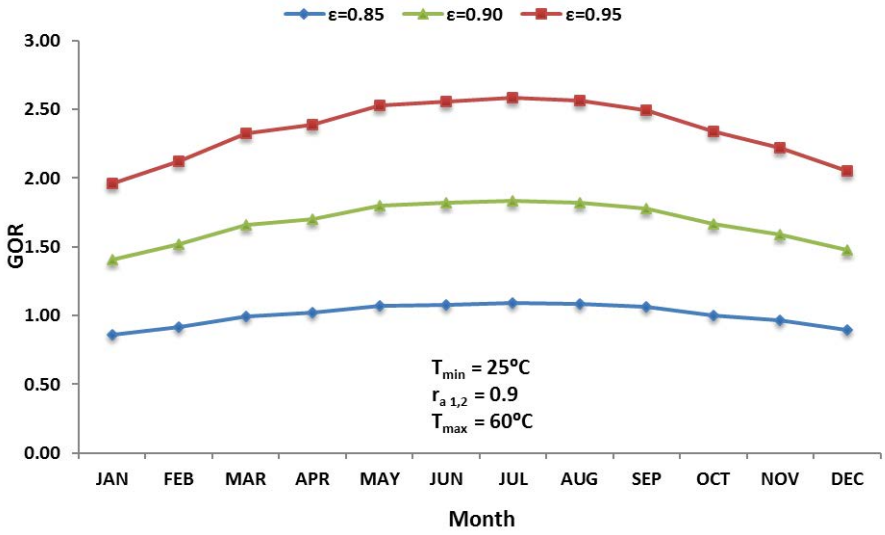

Fig. 10. Variation of the daily averaged GOR over the course of the year.

faster. The flow rate across the storage tank is assumed to be constant in this study. An operating condition for the HDH system is that the system maintains the hot storage tank temperature at 60°C. When the storage temperature is greater than this value, the HDH system becomes operational and both the water flow pump and the blowers start running. The system stops all flow at 60°C or below, allowing the storage tank temperature to be maintained at 60°C as the only heat losses will be standby heat losses from the tank. The tank specifications show that it has a thermal resistance of R16, thereby allowing the calculation of the tank-area loss coefficient.

In order to determine whether the HDH system should be modified, the water flux condition mentioned by Sharqawy et al. [43] was used. The condition is used to find the humidifier cross-sectional area (CSA), with the water mass flux over the packing material assumed to vary between a minimum of 0.8 kg/s m^2 and a maximum of 4.2 kg/s m^2. An average design value assumed for the water flux is 1.5 kg/s m^2. The relationship is given by the following equation:

$$\text{Water Mass Flux} = \frac{\text{Mass flow rate of water}}{\text{Cross-sectional Area}} \tag{16}$$

The averaged mass flow rate of seawater in a direct system (without thermal storage) was found to be 0.045 kg/s, suggesting that a humidifier with a cross-sectional area of 0.03 m^2 is required. The maximum flow rate of 0.075 kg/s reached for the direct system was on mid-day of June. This flow rate was also used as the maximum attainable flow rate for the system equipped with a storage option, thereby reducing CSA to 0.018 m^2. Therefore, it is evident that the system with a storage option can use smaller humidifiers and dehumidifiers. The CSA of the smaller humidifier was then used to calculate the maximum and minimum flow rates for the storage tank as well as the ideal flow rate. Further calculation was performed maintaining the average flow found from the base case. The minimum flow rate used in the study is that required to maintain a 24-h operation. The flow rate associated with the tank was calculated by finding the required heat input for the HDH system in order to maintain the calculated values of the seawater inlet flow rate. Four different cases were considered as follows:

- 24-h operation – related to the minimum flow rate (0.024 kg/s)
- Ideal flow rate – 1.5 water flux (0.027 kg/s)
- Average flow – average flow rate from the base case (0.045 kg/s)
- Maximum flow rate – 4.2 water flux (0.075 kg/s)

Simulations were performed for the average day of each month to calculate the product output, hourly and daily averaged values of GOR, and to determine the number of operating hours plus the production rate for each hour, for the above-mentioned cases. As mentioned earlier, the system with thermal storage is expected to have a constant production rate due to the addition of the required heat to maintain a constant heat input. The performance for each individual case was compared for 4 months of the year, where the weather and solar radiation are significantly different from each other. The 4 months selected represent the four seasons, where March, June, September, and December were selected to represent spring, summer, autumn, and winter, respectively.

The freshwater production is expected to be constant, but the amount of water produced will change depending on the heat input from the thermal storage tank. Each case studied has a different freshwater output for each operating hour, which however, does not significantly vary with a change in radiation or ambient temperature. The variables affecting the number of hours of operation are mainly the flow rate associated with the storage tanks (heat input and output), available solar radiation, and the seawater flow rate of the HDH system, which are controlled by the amount of heat provided via the storage tank. The numbers of hours of operation, in the 4 months extracted from the figures are shown in Table 5 along with the amount of water produced

at each hour and the total productivity on an average day of each month.

The total averaged useful heat energy gained in each case on the average day of the month of the year is shown in Fig. 11. With high flow rates within the collector and tank loop, more energy is gathered and stored. As expected, the change in energy is significantly greater in the months with a high intensity of radiation, and it is considerably smaller in the months with a lower solar radiation. The higher flow rate within the storage tank loop increases the freshwater production considerably in the months with a higher intensity of radiation due to more energy being stored and released at any given operating time. The useful heat collected is maximum in June in all cases, where the highest value is reported for the case with the maximum flow. The recorded value for the total heat gained for the average day in June is 94 MJ. Similarly, due to the low level of solar radiation, the lowest useful heat total was recorded in December for all four cases. The minimum value recorded is 33 MJ, and it is almost constant in all cases considered. The variation in the collected energy corresponds to the variation of available solar radiation in the four seasons.

The variation of the tank temperature for each of these cases and the four seasonal months was also studied and the results are shown in Figs. 12–15. The curves in these figures show that the temperature change is non-linear and has a bell shape as expected. The tank temperature starts at 333 K and gradually increases as heat is added until the added heat is either equal to or less than the heat removed from the tank. The highest temperature gradients are shown in the summer month (Fig. 17) followed by March (Fig. 16) and September (Fig. 18) and the lowest in December (Fig. 19) as expected. The higher temperatures are attained at lower flow rates owing to the slower heat removal and the lower temperatures are at higher flow rates owing to faster heat removal. This is also due to the change in heat addition being comparatively smaller as compared with the change in heat removal. The maximum tank temperature (356.7 K) is reached in June in the case of the lowest seawater flow rate for 24-h operation due to reasons previously described. The maximum temperatures for March, September, and December are, 353.2, 351.5, and 344.1 K, respectively, where all recorded temperatures are for the same 24-h operation case.

3.4. Analysis for multiple locations

To determine the feasibility of the system, it is necessary to evaluate the performance of the proposed system at locations with varying weather conditions. Hence, multiple locations in Saudi Arabia were selected to determine the effect of the operating time on the performance of the system and the total freshwater output. The main parameters that affect the performance of the system are expected to be the solar radiation intensity, ambient temperature and the latitude of each location. Same values of system parameters used in the analysis for Dhahran, including the humidifier and dehumidifier effectiveness, and the relative humidity of air at the inlet and the exit of the humidifier are used and the saline inlet temperature is assumed to be constant at 25°C. The analysis was performed for the four cases considered in the previous section for Dhahran. Initially, the useful heat gained (Q_{in}) via the evacuated tube collectors was determined for the six selected locations, which represent different geographical regions of Saudi Arabia. The selected locations are as follows:

- Central Region – Riyadh
- Central Region (North) – Qassim
- Western Central Region – Jeddah
- Eastern Region – Dhahran
- Southern Region – Sharurah
- Western North Region – Tabuk

Fig. 16 shows the heat input to the system at each location. As the differences of the heat input among the four cases are within 5 MJ, only the results for the average flow case is depicted in the figure. The average flow case was selected as it provides an average value compared with all

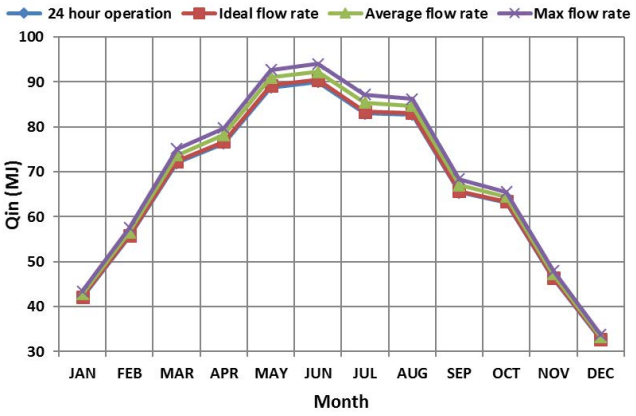

Fig. 11. Total useful energy collected for the average day of each month.

Table 5
Productivity and operating hours for four storage cases

Case	Freshwater (liters per hour)				No. of operating hours				Total freshwater productivity per day			
	Mar	Jun	Sep	Dec	Mar	Jun	Sep	Dec	Mar	Jun	Sep	Dec
24 h	3.0	3.0	3.0	3.0	23	24	24	22	69.2	72.2	72.2	66.2
Ideal flow	3.4	3.4	3.4	3.4	23	24	24	20	77.7	81.1	81.1	67.6
Average flow	5.6	5.6	5.6	5.6	17	19	18	15	95.5	106.7	101.1	84.2
Maximum flow	9.3	9.3	9.3	9.3	12	14	13	10	112.2	130.8	121.5	93.5

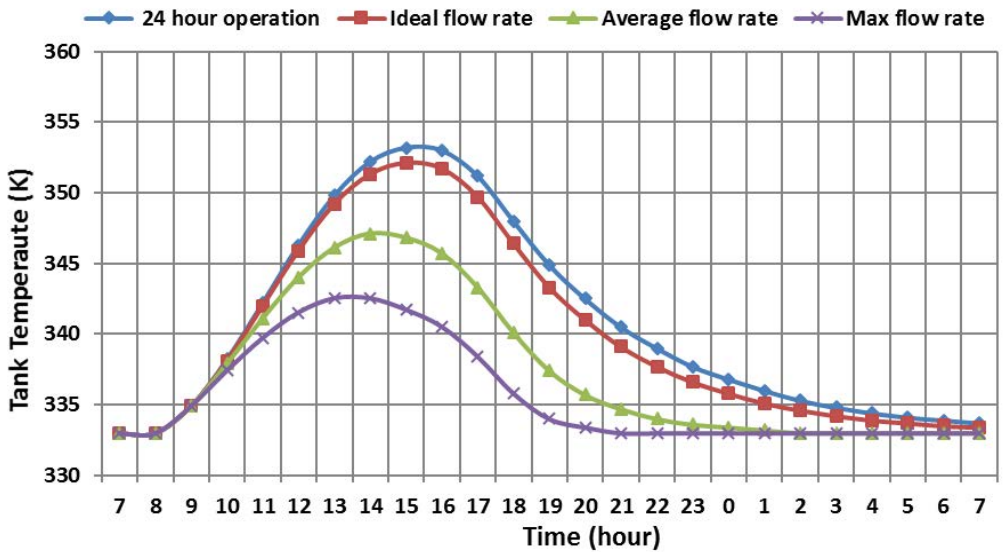

Fig. 12. Tank temperature variation for 24 hours (March).

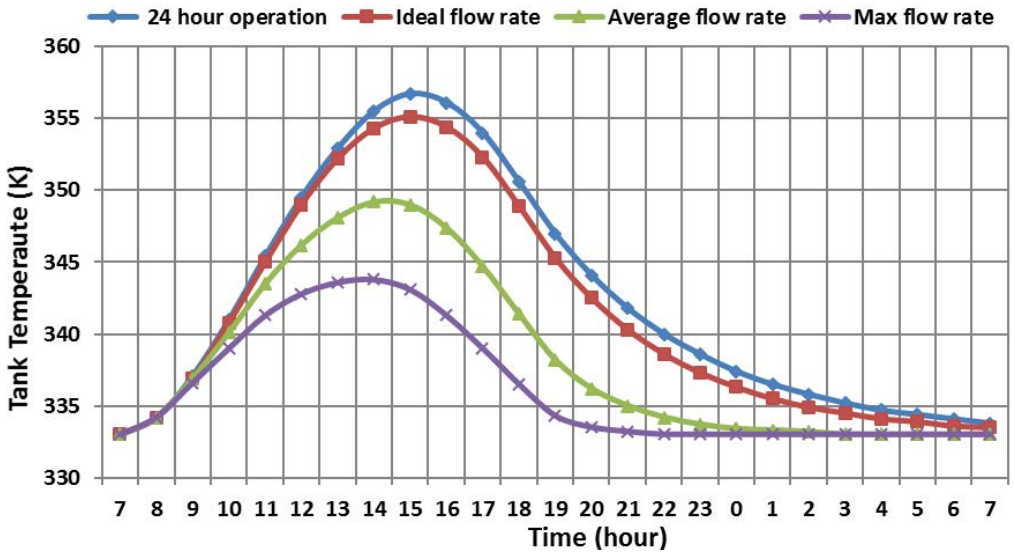

Fig. 13. Tank temperature variation for 24 h (June).

other cases. The figure shows that solar radiation at each city varies significantly from month to month.

It can be observed that the variation of solar radiation is considerably smaller during colder months such as January through March and October through December compared with warmer months. Qassim, Tabuk, and Riyadh have significantly higher radiation in the months of June, July, and August compared with other locations. Sharurah notably has considerably higher radiation values during the colder months mentioned above, and Tabuk has the lowest radiation levels during the same period.

The largest observed variation is in April, where Sharurah and Qassim have the maximum and minimum heat gained values, respectively. Heat gained is directly proportional to the availability of solar radiation as the system being evaluated only uses solar energy as a heat source. Hence, a high heat input value would generally suggest a relatively high solar radiation value. The data used in this comparison are the monthly averaged data for the year 2014. Various weather conditions may also affect the readings in turn affecting the radiation data. Therefore, some of the effects shown in the figure may well be due to significant changes in weather patterns during certain months at given locations (e.g., cloudy skies, rainy weather, dust storms, etc.). Fig. 16 can also be used as a reference to compare the operating hours of the systems as well as the total freshwater output. A higher heat input would suggest a relatively higher total freshwater output, a longer operating time as well as a higher storage tank temperature.

Tables 6 and 7 present results calculated for the four cases considering the conditions prevailing in typical locations of Riyad and Dhahran. The tables show the amount of

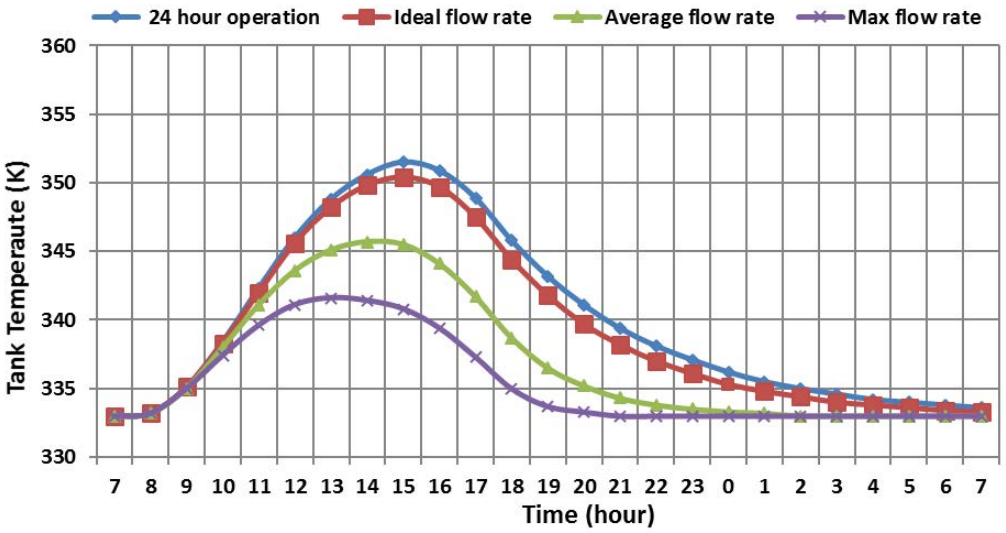

Fig. 14. Tank temperature variation for 24 h (September).

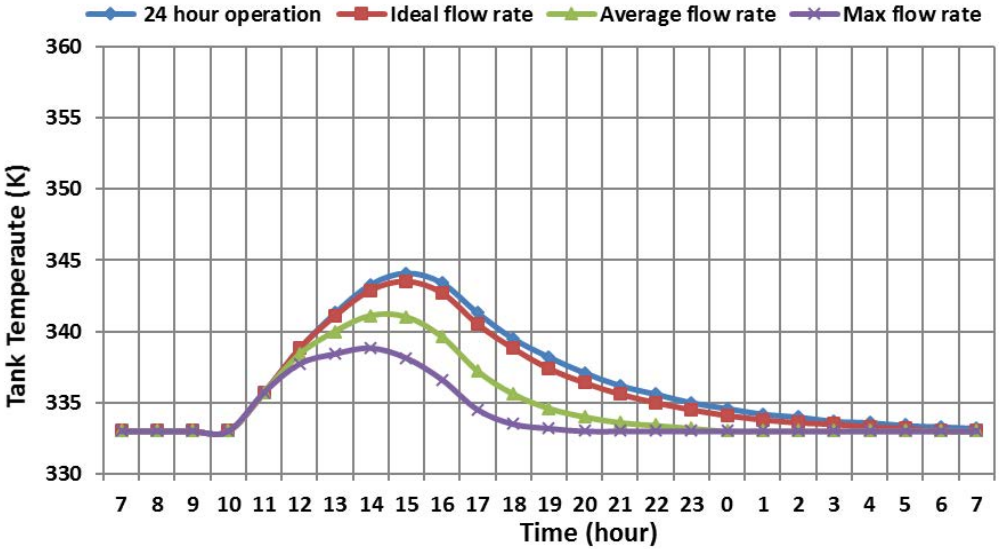

Fig. 15. Tank temperature variation for 24 h (December).

freshwater produced at each hour for the four cases along with the number of operating hours. These two parameters were then used to calculate the total productivity for the average day of the month for a complete year, which is also shown in the tables. The main parameter that varies among the different locations is the number of operating hours. However, the product per hour is not expected to change due to reasons discussed previously. The ambient temperature and the availability of solar radiation determine the operating hours at each location. As the ambient temperature only determines the losses from the system, if the system is well insulated and the storage tank standby losses are considerably low, the effect of the ambient temperature is quite low.

As the number of hours of operation is increased, more heat is added to the system, increasing the total daily productivity. This also means a greater availability of solar energy and longer hours of operation at locations that have a higher availability of solar radiation.

The total annual production of freshwater for the four cases at the six selected locations is shown in Table 8. The maximum flow case has the highest productivity, the reasons which were explained previously. The variation of freshwater production in the 24-h and ideal flow cases is quite low or sometimes insignificant as the number of hours of operation remains constant. However, large variations of production are observed for the average flow and maximum flow cases. The number of operating hours for these two cases varies depending on the location and for the maximum flow case Riyadh has the highest freshwater production followed by Sharurah, Dhahran, Jeddah, Qassim, and Tabuk. For the average flow case, the highest freshwater

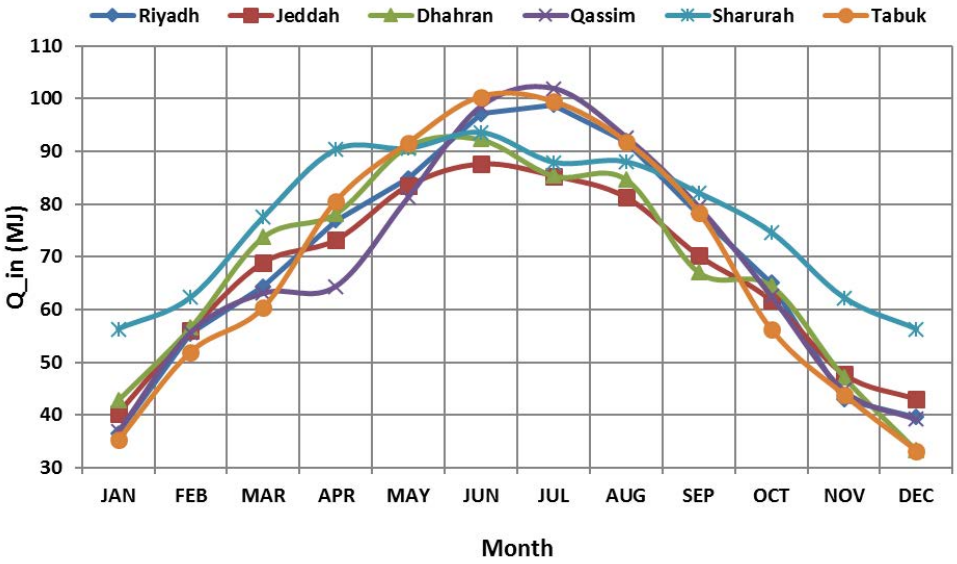

Fig. 16. Heat input over the entire duration of the year at selected locations.

Table 6
Operating hours and daily total freshwater production (Riyadh)

Month	Freshwater (liters per hour)				No. of operating hours				Total freshwater productivity per day			
	24-h	Ideal flow	Average flow	Maximum flow	24-h	Ideal flow	Average flow	Maximum flow	24-h	Ideal flow	Average flow	Maximum flow
Jan	3.0	3.4	5.6	9.3	23	22	15	11	69.2	74.3	84.2	102.8
Feb	3.0	3.4	5.6	9.3	23	23	16	11	69.2	77.7	89.9	102.8
Mar	3.0	3.4	5.6	9.3	24	24	17	13	72.2	81.1	95.5	121.5
Apr	3.0	3.4	5.6	9.3	24	24	18	13	72.2	81.1	101.1	121.5
May	3.0	3.4	5.6	9.3	24	24	18	13	72.2	81.1	101.1	121.5
Jun	3.0	3.4	5.6	9.3	24	24	19	14	72.2	81.1	106.7	130.8
Jul	3.0	3.4	5.6	9.3	24	24	19	14	72.2	81.1	106.7	130.8
Aug	3.0	3.4	5.6	9.3	24	24	18	14	72.2	81.1	101.1	130.8
Sep	3.0	3.4	5.6	9.3	24	24	18	13	72.2	81.1	101.1	121.5
Oct	3.0	3.4	5.6	9.3	24	24	18	13	72.2	81.1	101.1	121.5
Nov	3.0	3.4	5.6	9.3	23	22	15	11	69.2	74.3	84.2	102.8
Dec	3.0	3.4	5.6	9.3	23	22	15	11	69.2	74.3	84.2	102.8

production is at Sharurah followed by Dhahran, Riyadh, Jeddah, Tabuk, and Qassim. The differences between the two cases are mainly due to the amount of heat gained at a given hour. Although a case with a controlled flow rate would gain slightly less heat, it also uses considerably less heat to produce freshwater. Even though there is a greater heat gain at a given hour in the maximum flow case, the energy is lost instantly with the production of freshwater at each hour.

The maximum tank temperatures are shown in Table 9 for Riyadh. As expected, the temperature increases with increasing availability of solar energy as more useful heat is gained. The trend of the maximum tank temperature follows a similar trend to that of the heat input shown earlier in this section. The summer months of June or July have the highest recorded temperature. The lowest temperatures are recorded in the winter months, namely the months of January and December, where the days are shorter and solar radiation intensity is significantly lower compared with the rest of the year. The highest tank temperatures for the average flow case (350.1 K) and the maximum flow case (344.4 K) were recorded. The above results prove that the amount of freshwater produced, or the tank temperature do not depend only on the availability of solar energy, although an increase is observed with increased irradiation.

3.5. Cost analysis

The main objective of the cost analysis for the proposed system is to study the feasibility of the system in terms of the capital cost and the cost of water produced. The capital cost of a typical desalination plant includes items such as

Table 7
Operating hours and daily total freshwater production (Dhahran)

Month	Freshwater (liters per hour)				No. of operating hours				Total freshwater productivity per day			
	24-h	Ideal flow	Average flow	Maximum flow	24-h	Ideal flow	Average flow	Maximum flow	24-h	Ideal flow	Average flow	Maximum flow
Jan	3.0	3.4	5.6	9.3	22	21	15	10	66.2	71.0	84.2	93.5
Feb	3.0	3.4	5.6	9.3	23	23	16	12	69.2	77.7	89.9	112.2
Mar	3.0	3.4	5.6	9.3	23	23	17	12	69.2	77.7	95.5	112.2
Apr	3.0	3.4	5.6	9.3	24	24	18	13	72.2	81.1	101.1	121.5
May	3.0	3.4	5.6	9.3	24	24	19	14	72.2	81.1	106.7	130.8
Jun	3.0	3.4	5.6	9.3	24	24	19	14	72.2	81.1	106.7	130.8
Jul	3.0	3.4	5.6	9.3	24	24	19	14	72.2	81.1	106.7	130.8
Aug	3.0	3.4	5.6	9.3	24	24	19	14	72.2	81.1	106.7	130.8
Sep	3.0	3.4	5.6	9.3	24	24	18	13	72.2	81.1	101.1	121.5
Oct	3.0	3.4	5.6	9.3	24	24	17	12	72.2	81.1	95.5	112.2
Nov	3.0	3.4	5.6	9.3	23	23	15	11	69.2	77.7	84.2	102.8
Dec	3.0	3.4	5.6	9.3	22	20	15	10	66.2	67.6	84.2	93.5

Table 8
Total annual production of freshwater at the six locations for the four cases

Location	Annual productivity (L)			
	24-h	Ideal flow	Average flow	Maximum flow
Riyadh	23,960.5	26,684.6	32,704.9	39,910.4
Jeddah	23,960.5	26,785.9	32,530.8	39,050.6
Dhahran	23,770.9	26,569.7	32,879.0	39,583.3
Qassim	23,587.3	26,262.2	32,008.5	38,452.4
Sharurah	23,960.5	26,894.1	33,053.1	39,592.6
Tabuk	23,773.9	26,576.4	32,182.6	38,153.3

Table 9
Maximum tank temperatures for Riyadh

Month	Maximum storage temperature (K)			
	24-h	Ideal flow	Average flow	Maximum flow
Jan	344.4	343.8	341.3	338.7
Feb	349.5	348.6	344.8	341.1
Mar	351.4	350.4	345.9	341.8
Apr	353.6	352.4	347.3	342.6
May	354.9	353.6	348	343.1
Jun	357.4	356	349.7	344.2
Jul	357.9	355.6	350.1	344.4
Aug	356.8	355.4	349.4	344
Sep	354.1	352.9	347.7	342.9
Oct	351.7	350.6	346.2	341.9
Nov	346.1	345.4	342.4	339.5
Dec	345.3	344.7	341.9	339.2

the cost of land, supply well, equipment cost such as that for piping, tanks, pumps, etc., and building cost if indoor space is required. The cost will also include shipping, construction, services, etc.

Considering the current system, land costs may be ignored assuming outdoor location and operating in a rural deserted area. Thus, the cost of the equipment is the major cost item for a plant based on the HDH system. In addition, the required technical knowhow to setup a small plant based on the proposed design is low. Thus, the service or construction costs that must be incurred are minimal. The electricity consumption is expected to incur a negligible cost, which also may be acquired through photovoltaic technology without incurring running costs. This system may also be assumed to operate for 20 years without major maintenance. The cost of freshwater produced is calculated based on the procedure presented by Deniz and Çınar [42]. Some of the parameters involved in the calculation includes capital cost (P), sinking fund factor (SFF), annual salvage value (ASV), annual maintenance cost (AMC), and annual interest rate (i). The capital recovery factor, CRF is given as follows [48]:

$$\mathrm{CRF} = \frac{i(1+i)^n}{(1+i)^n - 1} \tag{17}$$

where n is the lifetime (year).

The fixed annual cost (FAC) is given as:

$$\mathrm{FAC} = P(\mathrm{CRF}) \tag{18}$$

The salvage value (S) is taken as 20% of the capital cost (P) [42]. Hence, sinking fund factor (SFF), annual salvage value (ASV) are, respectively, given as:

$$\mathrm{SFF} = \frac{i}{(1+i)^n - 1} \tag{19}$$

$$\mathrm{ASV} = S(\mathrm{SFF}) \tag{20}$$

Therefore, the total annual cost of the system is given as follows:

$$\mathrm{AC} = \mathrm{FAC} + \mathrm{ASV} + \mathrm{AMC} \tag{21}$$

The cost of fresh water (CFW) per liter is, therefore, calculated as:

$$\mathrm{CFW} = \frac{\mathrm{AC}}{\mathrm{AN}} \tag{22}$$

where AN is the annual output in liters. This system is also not expected to incur significant operational or maintenance costs.

The results obtained for each of these cases studied under the proposed design is given in Table 10. The list of capital costs incurred is shown in Table 11. The cost of purchasing a packaged solar system with a storage tank is around $4,000 cheaper than if components are purchased individually.

The cost of freshwater produced per liter using the proposed system (0.021 $/L) considering interest rate of 2% [49,50] seems to be high as compared with the price of freshwater in Saudi Arabia. However, when the cost of transporting water to rural areas, or areas not served by pipe-borne water is considered, the cost of water increases considerably because of transportation costs. Considering that the proposed system is being designed for such areas, the cost of water can be justified. The cost of the collectors and the storage tank as a packaged system with a heat exchanger may appear quite expensive at a first glance. However, this cost can be justified considering the quality and performance of the products manufactured by Apricus, which allow the recommendation of a service life of 20 years without major maintenance requirements and operational costs. In addition, the cost of solar collectors is expected to decrease in the near future and therefore, the associated cost of freshwater could be reduced. Although currently cheaper collector systems may be considered with the aim of reducing the cost of freshwater, when the service life and performance are factored in, the option may not be cost effective. The use of cheaper collector systems may also incur operational costs and require regular maintenance of the system, requiring the regular attention of a technician which may not be practical in rural areas.

Table 10
Cost per liter of water produced

Case	Annual output	Capital cost ($)	Cost/L ($)
			i = 2%
Maximum flow rate	42,356	12,539.00	0.021
Average flow rate	35,375		0.025
Ideal flow rate	28,567		0.03
24-h operation	25,730		0.034

4. Conclusions

This paper presented performance and cost assessment of an HDH system driven by evacuated tube collectors as water heaters and a two-tank storage system. The proposed system allows the control of the heat output required to maintain the desired temperature, thereby allowing the system to use less energy while maintaining it for a longer period. The following are the findings of the study:

- Higher flow rates mean faster heat addition and removal, whereas lower flow rates store slightly less heat but use less heat to produce fresh water, thereby increasing the operating time.
- The total daily output of a direct system is about 40 L/d on the average, whereas with storage it varies from around 70–130 L/d using the same number of evacuated tube collectors.
- Higher storage tank temperatures were attained with lower flow rates and considerably lower temperatures were attained with higher flow rates.
- The system had longer operating hours for locations with higher solar radiation intensity or longer hours of daylight and lower productivity for locations with shorter days or lower radiation intensities.
- For the maximum flow case, Riyadh has the highest freshwater production followed by Sharurah, Dhahran, Jeddah, Qassim, and Tabuk. For the average flow case,

Table 11
Cost of a packaged system and individual components

Item	Unit price ($)	Quantity	Price ($)
2xAP-30 + SOLX-120 Packaged system	8,461.00	1	8,461.00
AP-30 Mid-angle frame	219.00	2	438.00
Ducts	700.00	1	700.00
2 Tanks	475.00	2	950.00
Packing	750.00	1	750.00
Dehumidifier	500.00	1	500.00
2 Blowers	250.00	2	500.00
Additional pump	240.00	1	240.00
Total			12,539.00

the highest freshwater production is at Sharurah followed by Dhahran, Riyadh, Jeddah, Tabuk, and Qassim. The differences between the two cases are mainly due to the amount of heat gained at a given hour.

- The cost analysis suggests that the cost of freshwater produced vary from 0.021 to 0.034 $/L for a service life of 20 years considering interest rate of 2%.

Based on the results of this study, it is recommended to use the average flow case due to its higher freshwater productivity and almost 16 h of operation. As the system will not be operating for prolonged hours, system components such as pumps and fans can be operated with solar panels providing the required electricity using batteries to store the additional energy generated during daylight hours of the day.

Acknowledgments

The authors acknowledged the support of King Fahd University of Petroleum & Minerals (KFUPM), Dhahran, Saudi Arabia, for this work through the project IN131041. The authors also acknowledged the thesis work of Zubair "Thermal and economic analysis of HDH systems driven by solar thermal energy with a storage option" and the support of the Center of Research Excellence in Renewable Energy, KFUPM, Dhahran, Saudi Arabia.

Symbols

A_r	—	Area of the receiver, m^2
C_p	—	Heat capacitance of the working fluid, kJ/kg K
C_{pw}	—	Specific heat capacitance of water, kJ/kg K
CSA	—	Cross sectional area, m^2
F'	—	Collector efficiency factor
F_R	—	Collector heat removal factor
g	—	Gravitational acceleration
h_{a1}	—	Enthalpy of air at exit of the dehumidifier or the inlet of the humidifier, kJ/kg
h_{a2}	—	Enthalpy of air at the exit of the humidifier or the inlet of the dehumidifier, kJ/kg
h_{cond}	—	Heat transfer coefficient of the condenser, kJ/kg
h_{lh}	—	Enthalpy of latent heat, kJ/kg
h_{fg}	—	Enthalpy of latent heat of vaporization of water, kJ/kg
h_{fw}	—	Enthalpy of freshwater leaving the dehumidifier, kJ/kg
h_{hp}	—	Heat transfer coefficient of the heat pipe
h_{w1}	—	Enthalpy of the water entering the dehumidifier, kJ/kg
h_{w2}	—	Enthalpy of water at the exit of the dehumidifier, kJ/kg
h_{w4}	—	Enthalpy of brine at the exit of the humidifier, kJ/kg
I	—	Incident radiation on the horizontal surface, MJ/m^2
I_b	—	Fraction of beam radiation in a given hour, MJ/m^2
I_d	—	Fraction of diffused radiation in a given hour, MJ/m^2
I_T	—	Total radiation available to the collector, MJ/m^2
k_{cond}	—	Conductivity of the condenser, W/m K
k_{evap}	—	Evaporator conductivity, W/m K
k_{fin}	—	Conductivity of the fin, W/m K
k_l	—	Conductivity of the working fluid, W/m K
k_{ma}	—	Conductivity of the manifold, W/m K
k_v	—	Conductivity of vapor in the condenser, W/m K
L_{cond}	—	Length of the condenser, m
L_{evap}	—	Length of the evaporator, m
L_{ma}	—	Manifold length, m
m	—	Mass capacity of the storage tank, kg
m	—	Mass flow rate of the working fluid, kg/s
m_a	—	Mass flow rate of air, kg/s
m_b	—	Mass flow rate of brine, kg/s
m_{fw}	—	Mass flow rate of fresh water, kg/s
m_w	—	Mass flow rate of sea water, kg/s
Q	—	Energy input by the water heater, W
Q_u	—	Useful heat gained by the collector, W
R_b	—	Geometric factor for beam radiation
$R_{cond,w}$	—	Condenser wall thermal resistance, W/K
R_d	—	Geometric factor for diffused radiation
R_{gr}	—	Geometric factor for ground reflected radiation
R_{hp}	—	Evaporator (heat pipe) thermal resistance, W/K
$R_{loss,rad}$	—	Radiation thermal resistance, W/K
R_{ma}	—	Manifold resistance, W/K
S	—	Absorbed radiation, MJ/m^2
T_a	—	Ambient temperature, K
T_a'	—	Ambient temperature of the area surrounding storage tank, K
T_f	—	Temperature of the working fluid, K
T_i	—	Fluid inlet temperature, K
T_k	—	Temperature at the condenser wall, K
T_{Lr}	—	Load range temperature, K
T_o	—	Outlet temperature, K
T_p	—	Plate temperature, K
T_s^+	—	Temperature of storage at the end of the time period, K
T_{w2}	—	Temperature of water before the heater, K
T_{w3}	—	Water temperature at the exit of the water heater, K
U_L	—	Overall loss coefficient, W/m^2 K
U_{ma}	—	Manifold loss coefficient, W/m^2 K

Greek

$(UA)_s$	—	Storage tank loss coefficient-area product, kJ/h K
$(\tau\alpha)_b$	—	Transmittance–absorptance product for beam radiation
$(\tau\alpha)_d$	—	Transmittance–absorptance product for diffused radiation
$(\tau\alpha)_{gr}$	—	Transmittance–absorptance product for ground reflected radiation
μ_l	—	Viscosity of the working fluid, m^2/s
Δt	—	Length of the time period for which the calculations are carried out
ε	—	Emissivity of the absorber coating
ε_L	—	Load heat exchanger effectiveness
θ	—	Angle of incidence
ρ_{gr}	—	Ground reflectance
ρ_l	—	Density of the liquid within the evaporator, kg/m^3

ρ_v — Density of vapor in the condenser, kg/m^3
σ — Stefan–Boltzmann constant
ω_1 — Absolute humidity of air at the exit of the dehumidifier and the inlet of the humidifier, kg/m^3
ω_2 — Absolute humidity of air at the exit of the humidifier and the inlet of the dehumidifier, kg/m^3

References

[1] A. Chafidz, E.D. Kerme, I. Wazeer, Y. Khalid, A. Ajbar, S.M. Al-Zahrani, Design and fabrication of a portable and hybrid solar-powered membrane distillation system, J. Cleaner Prod., 133 (2016) 631–647.
[2] GWI, IDA Desalination Yearbook - 2015-2016, 2016. Available at: http://idadesal.org/.
[3] H.T. El-Dessouky, H.M. Ettouney, Fundamentals of Salt Water Desalination, Elsevier, 2002.
[4] A.E. Kabeel, M. Abdelgaied, A. Eisa, Enhancing the performance of single basin solar still using high thermal conductivity sensible storage materials, J. Cleaner Prod., 183 (2018) 20–25.
[5] G.P. Narayan, M.H. Sharqawy, E.K. Summers, J.H. Lienhard, S.M. Zubair, M.A. Antar, The potential of solar-driven humidification–dehumidification desalination for small-scale decentralized water production, Renew. Sustain. Energy Rev., 14 (2010) 1187–1201.
[6] R. Tripathi, G. Tiwari, Effect of water depth on internal heat and mass transfer for active solar distillation, Desalination, 173 (2005) 187–200.
[7] G. Wu, C. Kutlu, H. Zheng, Y. Su, D. Cui, A study on the maximum gained output ratio of single-effect solar humidification-dehumidification desalination, Sol. Energy, 157 (2017) 1–9.
[8] R. Santosh, T. Arunkumar, R. Velraj, G. Kumaresan, Technological advancements in solar energy driven humidification-dehumidification desalination systems - a review, J. Cleaner Prod., 207 (2019) 826–845.
[9] F.A. Al-Sulaiman, M.I. Zubair, M. Atif, P. Gandhidasan, S.A. Al-Dini, M.A. Antar, Humidification dehumidification desalination system using parabolic trough solar air collector, Appl. Therm. Eng., 75 (2015) 809–816.
[10] A.H.M.A. Hassabou, Experimental and Numerical Analysis of a PCM-Supported Humidification-Dehumidification Solar Desalination System, Technische Universität München, 2011.
[11] X. Huang, Y. Li, T. Ke, X. Ling, W. Liu, Thermal investigation and performance analysis of a novel evaporation system based on a humidification-dehumidification process, Energy Convers. Manage., 147 (2017) 108–119.
[12] J. Wang, N. Gao, Y. Deng, Y. Li, Solar power-driven humidification–dehumidification (HDH) process for desalination of brackish water, Desalination, 305 (2012) 17–23.
[13] P. Byrne, L. Fournaison, A. Delahaye, Y. Ait Oumeziane, L. Serres, P. Loulergue, A. Szymczyk, D. Mugnier, J.-L. Malaval, R. Bourdais, H. Gueguen, O. Sow, J. Orfi, T. Mare, A review on the coupling of cooling, desalination and solar photovoltaic systems, Renew. Sustain. Energy Rev., 47 (2015) 703–717.
[14] Y. Kim, T. Seo, Thermal performances comparisons of the glass evacuated tube solar collectors with shapes of absorber tube, Renew. Energy, 32 (2007) 772–795.
[15] K.C. Ng, C. Yap, T.H. Khor, Outdoor Testing of Evacuated-Tube Heat-Pipe Solar Collectors, in Proc. Inst. Mech. Eng. Part E J. Process Mech. Eng., 2000, pp. 23–30.
[16] C. Yildirim, I. Solmuş, A parametric study on a humidification-dehumidification (HDH) desalination unit powered by solar air and water heaters, Energy Convers. Manage., 86 (2014) 568–575.
[17] M.A. Elkader, A. Aref, G.H. Moustafa, Y. Elhenawy, A theoretical and experimental study for a humidification-dehumidification (HD) solar desalination unit, Int. J. Water Resour. Arid Environ., 3 (2014) 108–120.
[18] A.E. Kabeel, E.M.S. El-Said, A hybrid solar desalination system of air humidification–dehumidification and water flashing evaporation: Part I. A numerical investigation, Desalination, 320 (2013) 56–72.
[19] A.E. Kabeel, E.M.S. El-Said, A hybrid solar desalination system of air humidification, dehumidification and water flashing evaporation: Part II. Experimental investigation, Desalination, 341 (2014) 50–60.
[20] A.E. Kabeel, E.M.S. El-said, A hybrid solar desalination system ofair humidification dehumidification and water flashing evaporation: a comparison among different configuration, Desalination, 330 (2013) 79–89.
[21] T. Rajaseenivasan, K. Srithar, Potential of a dual purpose solar collector on humidification dehumidification desalination system, Desalination, 404 (2017) 35–40.
[22] A.E. Kabeel, M.H. Hamed, Z.M. Omara, S.W. Sharshir, Experimental study of a humidification-dehumidification solar technique by natural and forced air circulation, Energy, 68 (2014) 218–228.
[23] M.H. Hamed, A.E. Kabeel, Z.M. Omara, S.W. Sharshir, Mathematical and experimental investigation of a solar humidification–dehumidification desalination unit, Desalination, 358 (2015) 9–17.
[24] A.A. Al-Farayedhi, N.I. Ibrahim, P. Gandhidasan, Condensate as a water source from vapor compression systems in hot and humid regions, Desalination, 349 (2014) 60–67.
[25] H. Xu, Y. Zhao, T. Jia, Y.J. Dai, Experimental investigation on a solar assisted heat pump desalination system with humidification-dehumidification, Desalination, 437 (2018) 89–99.
[26] D. Lawal, M. Antar, A. Khalifa, S. Zubair, F. Al-sulaiman, Humidification-dehumidification desalination system operated by a heat pump, Energy Convers. Manage., 161 (2018) 128–140.
[27] H. Zhang, J. Baeyens, G. Cáceres, J. Degrève, Y. Lv, Thermal energy storage: recent developments and practical aspects, Prog. Energy Combust. Sci., 53 (2016) 1–40.
[28] J.A. Duffie, W.A. Beckman, Solar Engineering of Thermal Processes, 4th ed., John Wiley & Sons, 2013.
[29] A.A. Shabaneh, P. Gandhidasan, M.A. Antar, H. Baig, Simulation of HDH Desalination System Using Tilted, Two-Pass Solar Air Heater, in: Fifteenth International Water Technology Conference, 2011.
[30] E.K. Summers, M.A. Antar, J.H. Lienhard, Design and optimization of an air heating solar collector with integrated phase change material energy storage for use in humidification–dehumidification desalination, Sol. Energy, 86 (2012) 3417–3429.
[31] S. Xu, X. Ling, H. Peng, Experimental of New Thermal Storage in a Desalination System, Appl. Mech. Mater., 143–144 (2011) 531–535.
[32] Z. Wang, F. Qiu, W. Yang, X. Zhao, Applications of solar water heating system with phase change material, Renew. Sustain. Energy Rev., 52 (2015) 645–652.
[33] O. Miyatake, Y. Koito, K. Tagawa, Y. Maruta, Transient characteristics and performance of a novel desalination system based on heat storage and spray flashing, Desalination, 137 (2001) 157–166.
[34] S.M. Shalaby, M.A. Bek, A.E. Kabeel, Design Recommendations for Humidification-dehumidification Solar Water Desalination Systems, Energy Procedia, 107 (2017) 270–274.
[35] H. Müller-Holst, M. Engelhardt, W. Schölkopf, Small-scale thermal seawater desalination simulation and optimization of system design, Desalination, 122 (1999) 255–262.
[36] H. Muller-Holst, M. Engelhardt, M. Herve, W. Schijlkopf, Solar thermal sea water desalination systems for decentralised use, Renew. Energy, 14 (1998) 311–318.
[37] K.M. Abd El-Aziz, J. Kim, K. Hamza, M. El Morsi, A.O. Nassef, S.M. Metwalli, K. Saitou, Cost Optimization of a Solar Humidification-Dehumidification Desalination System Augmented by Thermal Energy Storage, in: ASME International Design Engineering Techical Conferences & Computers and Information in Engineering Conference, 2015, p. V02AT03A026. http://dx.doi.org/10.1115/DETC2015-46785.
[38] K. Srithar, T. Rajaseenivasan, Recent fresh water augmentation techniques in solar still and HDH desalination – a review, Renew. Sustain. Energy Rev., 82 (2018) 629–644.

[39] M.I. Zubair, Thermal and Economical Analysis of HDH Systems Driven by Solar Thermal Energy with a Storage Option, King Fahd University of Petroleum and Minerals, 2015. Available at: http://eprints.kfupm.edu.sa/139813/1/Thesis_-_M.I._Zubair_g201303430.pdf.
[40] M.I. Zubair, F.A. Al-sulaiman, M.A. Antar, S.A. Al-dini, N.I. Ibrahim, Performance and cost assessment of solar driven humidification dehumidification desalination system, Energy Convers. Manage., 132 (2017) 28–39.
[41] C. Yıldırım, İ. Solmuş, A parametric study on a humidification–dehumidification (HDH) desalination unit powered by solar air and water heaters, Energy Convers. Manage., 86 (2014) 568–575.
[42] E. Deniz, S. Çınar, Energy, exergy, economic and environmental (4E) analysis of a solar desalination system with humidification-dehumidification, Energy Convers. Manage., 126 (2016) 12–19.
[43] M.H. Sharqawy, M.A. Antar, S.M. Zubair, A.M. Elbashir, Optimum thermal design of humidification dehumidification desalination systems, Desalination, 349 (2014) 10–21.
[44] F. Jafarkazemi, H. Abdi, Evacuated tube solar heat pipe collector model and associated tests, J. Renew. Sustain. Energy, 4 (2012).
[45] Apricus, Product Catalog 2012 Sustainable Hot Water Solutions, 2012.
[46] Apricus 2015, Evacuated Tube Solar Collector, (n.d.). Available at: http://www.apricus.com/upload/userfiles/downloads/ETC_Collector_Overview_Int.pdf (Accessed 31 August 2016).
[47] G.P. Narayan, M.H. Sharqawy, J.H. Lienhard V, S.M. Zubair, Thermodynamic analysis of humidification dehumidification desalination cycles, Desal. Wat. Treat., 16 (2010) 339–353.
[48] B. Rahimi, J. May, A. Christ, K. Regenauer-Lieb, H.T. Chua, Thermo-economic analysis of two novel low grade sensible heat driven desalination processes, Desalination, 365 (2015) 316–328.
[49] A.M. Eltamaly, M.A. Mohamed, A.I. Alolah, A novel smart grid theory for optimal sizing of hybrid renewable energy systems, Sol. Energy, 124 (2016) 26–38.
[50] M.A. Mohamed, A.M. Eltamaly, A.I. Alolah, Swarm intelligence-based optimization of grid-dependent hybrid renewable energy systems, Renew. Sustain. Energy Rev., 77 (2017) 515–524.